1 **TITLE**

2 NLRC5 regulates expression of MHC-I and provides a target for anti-tumor immunity in

3 transmissible cancers

4 **RUNNING TITLE**

5 NLRC5 upregulates MHC-I on transmissible tumors

6 **AUTHORS**

7 Chrissie E. B. Ong[1*], Amanda L. Patchett[1], Jocelyn M. Darby[1], Jinying Chen[1,2], Guei-Sheung

8 Liu[1,3], A. Bruce Lyons[4], Gregory M. Woods[1], Andrew S. Flies[1*]

9 **AFFILIATIONS**

10 [1]Menzies Institute for Medical Research, College of Health and Medicine, University of

11 Tasmania, Hobart, TAS, Australia

12 [2]Department of Ophthalmology, the First Affiliated Hospital of Jinan University, Guangzhou,

13 China

14 [3]Ophthalmology, Department of Surgery, University of Melbourne, East Melbourne,

15 Australia

16 [4]Tasmanian School of Medicine, College of Health and Medicine, University of Tasmania,

17 Hobart, TAS, Australia

18 **CORRESPONDING AUTHORS CONTACT INFORMATION**

19 **Andrew S. Flies, PhD**

20 Menzies Institute for Medical Research, College of Health and Medicine

21 University of Tasmania

22 Private Bag 23, Hobart TAS 7000

23 phone: +61 3 6226 4614; email: Andy.Flies@utas.edu.au

24 **Chrissie E. B. Ong, PhD candidate**

25 Menzies Institute for Medical Research, College of Health and Medicine

26 University of Tasmania

27 Private Bag 23, Hobart TAS 7000

28 email: Chrissie.Ong@utas.edu.au

29 **KEYWORDS**

30 transmissible cancer, devil facial tumor, allograft, MHC-I, NLRC5, contagious cancer,

31 immune evasion, wild immunology

ABSTRACT

Downregulation of major histocompatibility complex I (MHC-I) on tumor cells is a primary means of immune evasion by many types of cancer. Additionally, MHC-I proteins are a primary target of immune-mediated transplant rejection. Transmissible tumors that overcome allograft rejection mechanisms and evade anti-tumor immunity have killed thousands of wild Tasmanian devils (*Sarcophilus harrisii*). Interferon gamma (IFNG) upregulates surface MHC-I expression on devil facial tumor (DFT) cells but is not sufficient to induce tumor regressions. Transcriptome analysis of IFNG-treated DFT cells revealed strong upregulation of *NLRC5*, a master regulator of MHC-I in humans and mice. To explore the role of NLRC5 in transmissible cancers, we developed DFT cell lines that constitutively overexpress NLRC5. Transcriptomic results suggest that the role of NLRC5 as a master regulator of MHC-I is conserved in devils. Furthermore, NLRC5 was shown to drive the expression of many components of the antigen presentation pathway. To determine if MHC-I is a target of allogeneic immune responses, we tested serum from devils with anti-DFT responses including natural DFT regressions against DFT cells. Antibody binding occurred with cells treated with IFNG and overexpressed NLRC5. However, CRISPR/Cas9-mediated knockout of MHC-I subunit beta-2-microglobulin (*B2M*) eliminated antibody binding to DFT cells. Consequently, MHC-I could be identified as a target for anti-tumor and allogeneic immunity and provides mechanistic insight into MHC-I expression and antigen presentation in marsupials. NLRC5 could be a promising target for immunotherapy and vaccines to protect devils from transmissible cancers and inform development of transplant and cancer therapies for humans.

INTRODUCTION

53   In 1996, a wild Tasmanian devil (*Sarcophilus harrisii*) was photographed with a large facial

54   In 1996, a wild Tasmanian devil (*Sarcophilus harrisii*) was photographed with a large facial

55   tumor. In subsequent years, similar devil facial tumors (DFTs) were recorded[1], and in 2006, it

56   was confirmed that DFTs are clonally transmissible cancers that spread among devils through

57   social interactions[2,3]. In 2014, a second genetically independent transmissible devil facial tumor

58   (DFT2) was discovered in southern Tasmania[4]. Despite the independent origin of the first devil

59   facial tumor (DFT1) and DFT2, both clonal tumors arose from a Schwann cell lineage[5,6],

60   suggesting devils could be prone to transmissible Schwann cell cancers. These lethal and

61   unique tumors are simultaneously cancers, allografts, and infectious diseases, and have been

62   the primary driver of an average 77% decline in devil populations across the island state of

63   Tasmania[7].

64

65   The successful transmission and seeding of DFT cells from one devil to another as an allograft[3]

66   reveals its ability to circumvent both allogeneic and anti-tumor immune responses. DFT1 cells

67   generally express little or no major histocompatibility complex class I (MHC-I) on their

68   surface[8], an immune escape mechanism commonly observed in human cancers[9] that prevents

69   recognition of tumor cells by cytotoxic anti-tumor CD8+ T cells. Beta-2-microglobulin (B2M)

70   is necessary for surface MHC-I expression and the clonal DFT1 cell lineage has a hemizygous

71   mutation in the *B2M* gene[10], suggesting that immune evasion through reduced MHC-I

72   expression has been a target of evolutionary selection pressure. Loss of MHC-I should lead to

73   recognition and cytotoxic responses by natural killer (NK) cells. Devils have demonstrated

74   NK-like activity *in vitro*[11] but the ongoing transmission of DFT1 cells suggests that NK

75   cytotoxic response against DFT1 cells either do not occur or are ineffective. All DFT1 cell

76   lines tested to date can upregulate MHC-I in response to interferon gamma (IFNG) treatment[8].

77   Rare cases of DFT1 regression have been reported in the wild[12] and serum antibody responses

78   of these devils are generally higher against cell lines treated with IFNG to upregulate MHC-

79   I[12,13]. In contrast to DFT1 cells, DFT2 cells constitutively express MHC-I, but the most highly-

80   expressed alleles appear to be those shared by the DFT2 cells and the host devil[14]. This further

81   suggest a critical role of MHC-I in immune evasion by DFT cells.

82

83   Upregulation of MHC-I on DFT1 cells via treatment with IFNG has served as the foundation

84   for a vaccine against devil facial tumor disease (DFTD), which is caused by DFT1 cells.

85   However, there are caveats to using a pleiotropic cytokine such as IFNG. IFNG plays multiple

86   roles in the innate and adaptive immune system and can function to drive either an anti-tumor

3

87 or a pro-tumor response depending on the circumstances[15]. While IFNG is well known for

88 directing the immune response towards anti-tumor immunity, it also causes the upregulation of

89 programmed death ligand 1 (PDL1)[16] and non-classical, monomorphic MHC-I SAHA-UK on

90 DFT cells[14]. PDL1 and SAHA-UK molecules can be counterproductive to the cell-mediated

91 immune response mediated by MHC-I recognition. Additionally, the inhibition of cell

92 proliferation and increased DFT cell death associated with IFNG[17] constrain large-scale

93 production of IFNG-treated DFT cells for whole cell vaccines.

94

95 NLRC5 (NLR caspase recruitment domain containing protein 5), a member of the NOD-like

96 receptor (NLR) family, was identified in 2010 as the transcriptional activator of MHC-I

97 genes[18]. NLRC5 is strongly upregulated by IFNG and is found to be a critical mediator for

98 IFNG-induced MHC-I expression in humans and mice[18], but little is known about NLRC5 in

99 other species. NLRC5 acts with high specificity[18], and functions in MHC-I regulation by

100 interacting with several other transcription factors[19] to form a multi-protein complex called the

101 enhanceosome[20,21]. The enhanceosome activates the promoters of MHC-I genes and

102 components of the antigen processing machinery such as B2M, immunoproteasome subunits

103 PSMB8 (also known as LMP7) and PSMB9 (also known as LMP2), and transporter associated

104 with antigen processing 1 (TAP1)[9,18]. Aside from MHC-I regulation, NLRC5 has been reported

105 to be involved in innate immune responses as well as malignancy of certain cancers[22]. Despite

106 a potential central role of NLRC5 in immune evasion, studies of NLRC5 remain limited and

107 several hypothesized secondary roles of NLRC5 remain unexplored[22].

108

109 In this study, we take advantage of a unique natural experiment in which two independent

110 clonal tumor cell lines have essentially been passaged through hundreds of free-living animals

111 to assess the role of NLRC5 and MHC-I in immune evasion. The overexpression of NLRC5 in

112 DFT1 and DFT2 cells induced the expression of *B2M*, MHC-I heavy chain *SAHAI-01* and other

113 functionally-related genes. *PDL1* and the non-classical MHC-I *SAHA-UK* which are

114 upregulated by IFNG were not induced by NLRC5. MHC-I was constitutively expressed on

115 the surface of DFT cells overexpressing NLRC5, which suggests that modulation of NLRC5

116 expression could be a potential substitute for IFNG to increase DFT cell immunogenicity.

117 Additionally, MHC-I molecules on DFT cells were revealed to be an immunogenic target of

118 allogeneic responses in wild devils.

119 **MATERIALS AND METHODS**

120 **Cells and Cell Culture Conditions**

121 DFT1 cell line C5065 strain 3[23] (RRID:CVCL_LB79) and DFT2 cell lines RV

122 (RRID:CVCL_LB80) and JV (RRID not available) were used in this study as indicated. DFT1

123 C5065 was provided by A-M Pearse and K. Swift of the Department of Primary Industries,

124 Parks, Water and Environment (DPIPWE) (Hobart, TAS, Australia) and was previously

125 established from DFT1 biopsies obtained under the approval of the Animal Ethics Committee

126 of the Tasmanian Parks and Wildlife Service (permit numbers 33/2004-5 and 32/2005-6).

127 DFT2 cell lines RV and JV were established from single cell suspensions obtained from tumor

128 biopsies[4]. Cells were cultured at 35 °C with 5% CO_2 in complete RPMI medium: RPMI 1640

129 medium with L-glutamine (Thermo Fisher Scientific, Waltham, MA, USA), 10% heat-

130 inactivated fetal bovine serum (Bovogen Biologicals, Melbourne, VIC, Australia), 1% (v/v)

131 Antibiotic-Antimycotic (100X) (Thermo Fisher Scientific), 10 mM HEPES (Thermo Fisher

132 Scientific) and 50 μM 2-mercaptoethanol (Sigma-Aldrich, St. Louis, MO, USA).

133

134 **RNA Sequencing and Analysis**

135 Initial RNA sequencing was performed using DFT1 C5065 and DFT2 RV cells treated with

136 and without 5 ng/mL recombinant devil IFNG (provided by Walter and Eliza Hall Institute

137 (WEHI), Melbourne, VIC, Australia) for 24 h according to the previously described

138 protocols[6,24]. For the remaining cell lines (**Table 1**, ID # 5–9), total RNA was extracted using

139 the NucleoSpin® RNA plus kit (Macherey Nagel, Düren, Germany) per manufacturer's

140 instructions. Two replicates were prepared for each cell line. RNA sequencing was conducted

141 at the Ramaciotti Centre for Genomics (Sydney, NSW, Australia) using the following methods.

142 RNA integrity was assessed using Agilent TapeStation (Agilent Technologies, Santa Clara, CA,

143 USA). All samples had RNA Integrity Number (RIN) scores of 10.0. mRNA libraries were

144 prepared using the TruSeq Stranded mRNA Library Prep (Illumina Inc., San Diego, CA, USA).

145 The libraries were sequenced on an Illumina NovaSeq 6000 platform (Illumina) with 100 base-

146 pair single-end reads. The quality of the sequencing reads were analyzed using FastQC version

147 0.11.9[25]. Raw FASTQ files have been deposited to the European Nucleotide Archive (ENA)

148 and are available at BioProject # PRJEB39847.

149

150 The sequencing reads were mapped to the Tasmanian devil reference genome

151 (GCA_902635505.1 mSarHar1.11) using Subread version 2.0.0[26]. Uniquely mapped reads

152 were counted and assigned to genes using featureCounts[27]. Differential expression analysis of

153 gene counts was performed using statistical software R studio[28] on R version 4.0.0[29]. Firstly,

154 genes with less than 100 aligned reads across all samples were filtered out to exclude lowly

155 expressed genes. Gene counts were then normalized across samples by upper quartile

156 normalization using edgeR[30–32] and EDASeq[33,34]. Normalized read counts were scaled by

157 transcripts per kilobase million (TPM) to account for varied gene lengths. For differential

158 expression analysis, gene expression of NLRC5-overexpressing cell lines (DFT1.NLRC5,

159 DFT2.NLRC5) were compared against BFP-control cell lines (DFT1.BFP, DFT2.BFP) while

160 IFNG-treated cells (DFT1.WT + IFNG, DFT2.WT^{RV} + IFNG) were compared against the

161 untreated wild-type (DFT1.WT, DFT2.WT^{RV}), according to their respective tumor origin.

162 Differential gene expression was calculated using the *voom*[35] function in *limma*[36] with linear

163 modelling and empirical Bayes moderation[37] (**Supplementary Table 1**). Genes were defined

164 as significantly differentially expressed by applying FDR < 0.05, and log$_2$ fold change (FC) ≥

165 2.0 (upregulated) or ≤ −2.0 (downregulated) thresholds.

166

167 A bar plot of fold change in mRNA expression upon treatment was created from TPM values

168 in GraphPad Prism version 5.03. Venn diagrams of differentially expressed genes were

169 developed using Venny version 2.1[38]. Heatmaps were created from log$_2$TPM values using the

170 ComplexHeatmap[39] package in R studio. For functional enrichment analysis, over-

171 representation of gene ontology (GO) and Reactome pathways was analyzed on differentially

172 expressed genes in R studio using functions *enrichGO* in ClusterProfiler[40] and *enrichPathway*

173 in ReactomePA[41], respectively. Significant GO terms and Reactome pathways were selected

174 by applying the cut-offs p-value < 0.001, q-value < 0.05 and adjusted p-value < 0.05. P-values

175 were adjusted for multiple testing using Benjamini–Hochberg method.

176

177 **Plasmid Construction**

178 The coding sequence for full length devil *NLRC5* (ENSSHAT00000015489.1) was isolated

179 from cDNA of devil lymph node mononuclear cells stimulated with recombinant devil IFNG[16]

180 (10 ng/mL, 24 h). Devil *NLRC5* was then cloned into plasmid pAF105 (detailed description of

181 pAF105 plasmid construction available in **Supplementary Methods 1**). For this study, devil

182 *NLRC5* was amplified from pAF105 with overlapping ends to the 5' and 3' SfiI sites of the

183 Sleeping Beauty transposon plasmid pSBbi-BH[42] (a gift from Eric Kowarz; Addgene # 60515,

184 Cambridge, MA, USA) using Q5$^{®}$ Hotstart High-Fidelity 2X Master Mix (New England

185 Biolabs (NEB), Ipswich, MA, USA) (see **Supplementary Table 2** for primers and reaction

6

186   conditions). The fragment was cloned into SfiI-digested (NEB) pSBbi-BH using NEBuilder®

187   HiFi DNA Assembly Cloning Kit (NEB) and the assembled plasmid pCO1 was transformed

188   into NEB® 5-alpha competent *Escherichia coli* (High Efficiency) (NEB) according to

189   manufacturer's instructions (see **Supplementary Figure 1** for plasmid maps). Positive clones

190   were identified by colony PCR and the plasmid was purified using NucleoSpin® Plasmid

191   EasyPure kit (Macherey-Nagel). The cloned devil *NLRC5* transcript was verified by Sanger

192   sequencing using Big Dye™ Terminator v3.1 Cycle Sequencing Kit (Applied Biosystems

193   (ABI), Foster City, CA, USA) and Agencourt® CleanSEQ® (Beckman Coulter, Brea, CA, USA)

194   per manufacturer's instructions. The sequences were analyzed on 3500xL Genetic Analyzer

195   (ABI) (see **Supplementary Table 3** for list of sequencing primers). For detailed step-by-step

196   protocols for plasmid design and construction, reagent recipes, and generation of stable cell

197   lines, see Bio-protocol # e3986[43].

198

199   **Transfection and Generation of Stable Cell Lines**

200   Stable cell lines of both DFT1 and DFT2 (C5065 and JV cell lines respectively) overexpressing

201   NLRC5 were prepared as follows. 5×10^5 cells were seeded into a 6-well plate and incubated

202   overnight to achieve 50–80% confluency on the day of transfection. As the vector constructed

203   uses a Sleeping Beauty (SB) transposon system for gene transfer, co-transfection of an

204   expression vector encoding a SB transposase enzyme pCMV(CAT)T7-SB100[44] (a gift from

205   Zsuzsanna Izsvak; Addgene plasmid # 34879) was needed to facilitate this process. Per 2.0 mL

206   of culture volume, 2.0 μg of plasmid DNA (1.5 μg pCO1 + 0.5 μg pCMV(CAT)T7-SB100)

207   was diluted in phosphate-buffered saline (PBS) to 100 μL and then added to 6.0 μg of

208   polyethylenimine (PEI) (1 mg/mL, linear, 25 kDa; Polysciences, Warrington, FL, USA) diluted

209   in PBS to 100 μL (3:1 ratio of PEI to DNA (w/w)). The DNA:PEI solution was mixed by gentle

210   pipetting and incubated at room temperature for 15 to 20 min. The media on DFT cells were

211   replaced with fresh complete RPMI medium and the transfection mix was added dropwise to

212   the cells. The cells were incubated with the DNA:PEI solution overnight at 35 °C with 5% CO_2.

213   The next morning, media was replaced with fresh complete RPMI medium. 48 h post-

214   transfection, the cells were observed for fluorescence through expression of reporter gene

215   mTagBFP and were subjected to seven days of positive selection by adding 1 mg/mL

216   hygromycin B (Sigma-Aldrich) in complete RPMI medium. Once selection was complete, the

217   cells were maintained in 200 μg/mL hygromycin B in complete RPMI medium. pSBbi-BH was

218   used as a control to account for the effects of the transfection and drug selection process.

7

Flow Cytometric Analysis of B2M Expression

Cells were harvested and plated in a round-bottom 96-well plate (1×10^5 per well) and centrifuged at 500g for 3 min at 4 °C to discard the medium. Cells were blocked with 50 μL of 1% normal goat serum (Thermo Fisher Scientific) in FACS buffer (PBS with 0.5% BSA, 0.02% sodium azide) for 10 min on ice. After blocking, 0.4 μL anti-devil B2M mouse antibody in supernatant (13-34-45, a gift from Hannah Siddle)[8] diluted to a total of 50 μL in FACS buffer was added to the cells for 15 min on ice. The cells were washed with 150 µL FACS buffer and centrifuged at 500g for 3 min at 4 °C. Goat anti-mouse IgG-Alexa Fluor 488 (Thermo Fisher Scientific) was diluted in FACS buffer to 4 µg/mL and 50 μL of the solution was incubated with the target cells in the dark for 30 min on ice. The cells were washed twice with FACS buffer to remove excess secondary antibody. Lastly, the cells were resuspended in 200 µL FACS buffer with propidium iodide (PI) (500 ng/mL) (Sigma-Aldrich) prior to analysis on BD FACSCanto[TM] II (BD Biosciences, Franklin Lakes, NJ, USA). As a positive control for surface B2M expression, DFT1 C5065 and DFT2 JV cells were stimulated with 5 ng/mL recombinant devil IFNG[16] for 24 h.

Generation of *B2M* CRISPR/Cas9 Knockout Cell Lines (B2M^{-/-})

Two single guide RNAs (sgRNAs) targeting the first exon of devil *B2M* gene (ENSSHAG00000017005) were designed using a web-based CRISPR design tool CHOPCHOP[45] (**Supplementary Figure 2**). Complementary oligonucleotides encoding each *B2M* sgRNA sequence were synthesized (Integrated DNA Technologies (IDT), Coralville, IA, USA), phosphorylated and annealed before cloning into lentiCRISPRv2 plasmid[46] (a gift from Feng Zhang; Addgene # 52961) at BsmBI (NEB) restriction sites using T4 DNA ligase (NEB) (see **Supplementary Table 4** for oligonucleotide sequences). The ligated plasmids pAF217 and pAF218 were then transformed into NEB[®] Stable Competent *Escherichia coli* (High Efficiency) (NEB). Single colonies were selected, and the plasmids were purified using ZymoPURE™ Plasmid Miniprep Kit (Zymo Research, Irvine, CA, USA). The sgRNA sequence in each plasmid was validated by Sanger sequencing according to the method described above (see **Supplementary Table 3** for list of sequencing primers).

B2M targeting vectors pAF217 and pAF218 were each transfected into DFT1.WT and DFT1.NLRC5 cells to generate *B2M* knockout cell lines DFT1.B2M^{-/-} and

8

252   DFT1.NLRC5.B2M$^{-/-}$. Transfection of cells were carried out as described above with the

253   exception that 1.5 μg of plasmid was used instead of 2.0 μg. A day after transfection, the cells

254   were subjected to positive selection by adding 100 μg/mL puromycin (InvivoGen, San Diego,

255   CA, USA) for a week.

256

257   Post-drug selection, the cells were screened and sorted multiple rounds using a Beckman-

258   Coulter MoFlo Astrios cell sorter to select DFT1.B2M$^{-/-}$ and DFT1.NLRC5.B2M$^{-/-}$ cells with

259   negative B2M expression. DFT1.B2M$^{-/-}$ cells were treated with 10 ng/mL devil recombinant

260   IFNG[16] for 24 h to stimulate surface B2M upregulation prior to analysis. For flow cytometry,

261   cells were first harvested by centrifugation at 500g for 3 min at 4 °C, and then blocked with

262   100 μL of 1% normal goat serum (Thermo Fisher Scientific) in complete RPMI medium for

263   10 min on ice. After blocking, the cells were incubated with 0.8 μL anti-devil B2M mouse

264   antibody in supernatant[8] diluted in complete RPMI to a total of 100 μL for 15 min on ice. The

265   cells were washed with 2.0 mL complete RPMI and centrifuged at 500g for 3 min at 4 °C. Next,

266   the cells were incubated with 100 μL of 2 μg/mL goat anti-mouse IgG-Alexa Fluor 647

267   (Thermo Fisher Scientific) diluted in complete RPMI in the dark for 15 min on ice. The cells

268   were washed with 2.0 mL of complete RPMI medium to remove excess secondary antibody.

269   Lastly, the cells were resuspended to a concentration of 1×10^7 cells/ml in 200 ng/mL DAPI

270   (Sigma-Aldrich) diluted in complete RPMI medium. B2M negative cells were selected and

271   bulk-sorted using cell sorter Moflo Astrios EQ (Beckman Coulter).

272

273   After multiple rounds of sorting to establish a B2M negative population, genomic DNA of the

274   cells was isolated and screened for mutations in the *B2M* gene by Sanger sequencing (see

275   **Supplementary Table 3** for sequencing primers). Indels (insertions or deletions) in the *B2M*

276   gene were assessed using Inference of CRISPR Edits (ICE) analysis tool version 2.0 from

277   Synthego[47] (Menlo Park, CA, USA) (**Supplementary Figure 2**). *B2M* knockout cell lines: (i)

278   DFT1.B2M$^{-/-}$ derived from DFT1 cells transfected with pAF217, and (ii) DFT1.NLRC5.B2M$^{-/-}$

279    $^{/-}$ derived from DFT1.NLRC5 transfected with pAF218 were selected for downstream analysis

280   (see **Table 1** for full list of cell lines).

281

282   **Flow Cytometric Analysis of Serum Antibody Target**

283   Serum samples from wild Tasmanian devils were collected as described[12,48]. To induce surface

284   expression of MHC-I, DFT cells were treated with 10 ng/mL devil recombinant IFNG[16] for 24

9

285   h prior to analysis. Cells were washed with cold FACS buffer and 1×10^5 cells per well were

286   plated in a round-bottom 96-well plate. The cells were centrifuged at 500g for 3 min at 4 °C to

287   discard the medium. Serum samples (see **Supplementary Table 5** for serum sample

288   information) were thawed on ice and diluted 1:50 with FACS buffer. 50 μL of diluted serum

289   was added to the cells and incubated for 1 h on ice. After incubation, the cells were washed

290   twice with 200 μL FACS buffer. 50 μL of 10 μg/mL monoclonal mouse anti-devil IgG2b

291   antibody (A4-D1-2-1, provided by WEHI)[49] in FACS buffer was added to the cells and

292   incubated for 30 min on ice. The cells were washed twice with FACS buffer and then incubated

293   with 50 µL of 4 μg/ml goat anti-mouse IgG-Alexa Fluor 488 (Thermo Fisher Scientific) in

294   FACS buffer for 30 min on ice, protected from light. The cells were washed twice with ice-

295   cold PBS (Thermo Fisher Scientific). After washing, the cells were stained with

296   LIVE/DEAD[TM] Fixable Near-IR Dead Cell Stain (Thermo Fisher Scientific) per

297   manufacturer's instructions. For B2M surface expression analysis, the cells were stained as

298   described in the protocol above. However, LIVE/DEAD[TM] Fixable Near-IR Dead Cell Stain

299   (Thermo Fisher Scientific) was used instead of PI to determine cell viability. All cells were

300   fixed with FACS fix (0.02% sodium azide, 1.0% glucose, 0.4% formaldehyde) diluted by 20

301   times prior to analysis on BD FACSCanto[TM] II (BD Biosciences).

302

303   **RESULTS**

304   **NLRC5 is upregulated in DFT1 and DFT2 cells treated with IFNG**

305   IFNG has been shown to upregulate MHC-I[8] and PDL1[16] on DFT cells. To probe the

306   mechanisms driving upregulation of these key immune proteins, we performed RNA-seq using

307   mRNA extracted from IFNG-treated DFT1 cell line C5065 (DFT1.WT) and an IFNG-treated

308   DFT2 cell line RV (DFT2.WT[RV]). Markers for Schwann cell differentiation, SRY-box 10

309   (SOX10) and neuroepithelial marker nestin (NES), that are expressed in both DFT1 and DFT2

310   cells[6], were selected as internal gene controls. As expected, transcriptome analysis showed that

311   *B2M*, MHC-I gene *SAHAI-01*, and *PDL1* were strongly upregulated by IFNG. MHC-I

312   transactivator *NLRC5* was also upregulated upon IFNG treatment, more than a 100-fold in

313   DFT1.WT (275-fold) and DFT2.WT[RV] cells (124-fold) relative to untreated cells (**Fig. 1**).

314

315   **NLRC5 upregulates MHC-I and antigen presentation genes but not PDL1 and non-**

316   **classical MHC-I**

10

317 To assess the role of NLRC5 in antigen processing and presentation, we developed an
318 expression vector that stably upregulates NLRC5 in DFT cells. DFT1 cell line C5065 and
319 DFT2 cell line JV were used for production of NLRC5-overexpressing DFT cells. Following
320 drug selection to create stable cell lines, we performed RNA-seq on DFT1 and DFT2 cells
321 stably transfected with BFP-control and NLRC5 vectors (see **Table 1** for list of cell lines).
322 Changes in the mRNA expression profile of DFT cells overexpressing NLRC5 relative to BFP-
323 control cells were examined in parallel with changes observed in wild-type DFT cells following
324 IFNG treatment (**Fig. 2** and **Supplementary Fig. 3**). The transcriptome for IFNG-treated DFT2
325 cells was previously generated from the DFT2 RV cell line (DFT2.WT^{RV})[6]. Otherwise, all
326 DFT2 results are from DFT2 JV.

327

328 Differential expression analysis showed that 159 genes were upregulated by IFNG (DFT1.WT
329 + IFNG) in contrast to 40 genes by NLRC5 (DFT1.NLRC5) in DFT1 cells (**Fig. 2**). In DFT2
330 cells, 288 genes were upregulated by IFNG (DFT2.WT^{RV} + IFNG) and 30 genes by NLRC5
331 (DFT2.NLRC5) (**Fig. 2**). There were ten genes that were upregulated by both IFNG and
332 NLRC5 in DFT1 and DFT2 cells. These shared genes were predominantly related to MHC-I
333 antigen processing and presentation pathway which suggests a role of NLRC5 in IFNG-
334 induced MHC-I expression.

335

336 A heatmap was used to explore the expression profiles of genes associated with MHC-I and
337 MHC-II antigen processing and presentation. SOX10 and NES, which are Schwann cell
338 differentiation markers highly expressed in DFT1 and DFT2 cells[6], and the myelin protein
339 periaxin (PRX), a marker for DFT1 cells[50], were included as internal controls. Overall, NLRC5
340 upregulated genes involved in MHC-I antigen presentation to a smaller magnitude than IFNG
341 (**Fig. 3**). NLRC5 upregulated a subset of IFNG-induced MHC-I genes *SAHAI-01*, *SAHAI*
342 *(LOC105750614)* and *SAHAI (LOC100927947)*, and genes of the antigen processing
343 machinery including *B2M*, *PSMB8*, *PSMB9*, and *TAP1*. In comparison, other IFNG-induced
344 genes such as *PSMB10*, *TAP2* and TAP binding protein (*TAPBP*) were not upregulated by
345 NLRC5 in either DFT1.NLRC5 or DFT2.NLRC5 cells. MHC-I genes that were induced by
346 IFNG but not NLRC5 include non-classical MHC-I genes *SAHA-UK* and *SAHA-MR1*, although
347 the latter was only induced in DFT2 cells treated with IFNG. Additionally, *PDL1* was
348 upregulated by IFNG, but not NLRC5. Examination of the promoter elements immediately
349 upstream of *SAHA-UK* and *PDL1* did not identify the putative MHC-I-conserved SXY
350 module[51] necessary for NLRC5-mediated transcription in the devil genome. A putative

11

351 interferon-stimulated response element (ISRE) for devil MHC-I genes was identified 127 bp

352 upstream of the start codon of *SAHA-UK* (**Supplementary Fig. 4**).

353

354 NLRC5 did not consistently regulate MHC-II genes. However, the invariant chain associated

355 with assembly of MHC-II complexes, *CD74*, was significantly upregulated in DFT1.NLRC5.

356 Similarly, IFNG treatment on DFT1 cells only upregulated MHC-II transactivator *CIITA*.

357 Strikingly, IFNG treatment on DFT2 cells induced several MHC-II genes such as *HLA-DRA*

358 *(LOC100923003)*, *HLA-DMA (LOC100925801)*, *HLA-DMB (LOC100925533)*, *CD74* and

359 *CIITA*.

360

361 **NLRC5 primarily functions in MHC-I antigen processing and presentation but is not**

362 **limited to immune-related functions**

363 The majority of research into NLRC5 has been devoted to its role as a regulator of MHC-I

364 expression. In addition, some studies have reported possible roles of NLRC5 in antiviral

365 immunity, inflammation and cancer through modulation of various signaling pathways[52–57]. To

366 identify additional biological functions of NLRC5 in DFT cells, over-representation analysis

367 of gene ontology (GO) biological processes and Reactome pathways was performed using the

368 list of differentially expressed genes between NLRC5-overexpressing DFT cells and BFP-

369 controls (FDR < 0.05, $\log_2$FC ≥ 2.0 or ≤ −2.0). Both analyses revealed significant up- and

370 downregulation of genes associated with immune system processes and developmental

371 processes in cells overexpressing NLRC5.

372

373 Among the list of genes upregulated in DFT1.NLRC5 and DFT2.NLRC5 cells, the most

374 significantly associated GO biological process was *antigen processing and presentation of*

375 *exogenous peptide antigen via MHC class I, TAP-dependent* (**Figs. 4A** and **5A**). Several

376 additional immune-related processes were also associated with NLRC5 overexpression,

377 particularly in DFT1 cells. Some of these included *positive regulation of immune response*,

378 *interferon-gamma-mediated signaling pathway*, *immune response-regulating cell surface*

379 *receptor signaling pathway* (**Fig. 4A**), and *regulation of interleukin-6 biosynthetic process*

380 (**Fig. 4C**). In DFT1.NLRC5 and DFT2.NLRC5, GO terms related to development that were

381 significantly over-represented included *morphogenesis of an epithelium* (**Fig. 4A)** and *negative*

382 *regulation of epidermis development* (**Fig. 5A**), respectively.

383

384   As DFT cells are of neuroendocrine origin, specifically of the Schwann cell lineage[5,6], a

385   number of neural-related genes were targeted by NLRC5. In DFT2 cells, NLRC5 upregulated

386   genes that are involved in *myelination*, which are usually expressed at low levels in DFT2 cells[6]

387   (**Fig. 5A**). These genes include brain enriched myelin associated protein 1 (*BCAS1*), myelin

388   binding protein (*MBP*), myelin protein zero (*MPZ*) and UDP glycosyltransferase 8 (*UGT8*)

389   (**Fig. 5B**). Furthermore, many of the downregulated genes in DFT2.NLRC5 were related to

390   nervous system function, mainly pertaining to *synaptic signaling* and *sensory perception* (**Fig.**

391   **5C**).

392

393   Reactome pathway analysis revealed an enrichment of pathways that were consistent with

394   those identified by GO analysis. This included enrichment of the *ER-phagosome pathway* and

395   *antigen processing-cross presentation* in DFT1.NLRC5 (**Table 2**) and DFT2.NLRC5 (**Table**

396   **3**); *signaling by the B cell receptor (BCR)* in DFT1.NLRC5; and *transmission across chemical*

397   *synapses* in DFT2.NLRC5 cells. Interestingly, nuclear factor of activated T cells 1 (*NFATC1*),

398   protein kinase C beta (*PRKCB*), *PSMB8* and *PSMB9*, associated with several GO immune-

399   related processes in DFT1.NLRC5 (**Fig. 4B**), were enriched for the *beta-catenin independent*

400   *WNT signaling* pathway (**Table 2**). Other enriched pathways included those involved in

401   extracellular matrix organization such as *collagen chain trimerization* (**Table 2**) and *assembly*

402   *of collagen fibrils and other multimeric structures* (**Table 3**).

403

404   **NLRC5 induces MHC-I expression on the cell surface**

405   To determine if NLRC5 is capable of regulating MHC-I expression at the protein level, surface

406   MHC-I was analyzed by flow cytometry in DFT cells overexpressing NLRC5 using a

407   monoclonal antibody against B2M[8]. The overexpression of NLRC5 induced upregulation of

408   surface expression of B2M in both DFT1.NLRC5 (**Fig. 6A**) and DFT2.NLRC5 cells (**Fig. 6B**).

409   The level of B2M expression was also comparable to wild-type DFT cells treated with IFNG.

410

411   Next, we assessed the stability of NLRC5-induced MHC-I expression by examining the

412   expression of B2M in long-term cultures. One-month post-drug selection, DFT1.NLRC5 cells

413   cultured in the presence or absence of hygromycin B were stained for B2M every four weeks

414   for a total of 12 weeks. As shown in **Fig. 6A**, MHC-I expression was stably maintained in

415   DFT1.NLRC5 cells, with or without ongoing drug selection pressure throughout the 12-week

416   culture thus, demonstrating the relative stability of the human EF1a promoter driving NLRC5

417   expression in long-term cell cultures. PDL1 was also not upregulated on the cell surface in

13

418   NLRC5-overexpressing DFT cells compared to IFNG-treated DFT cells (**Supplementary Fig.**

419   **5**).

420

421   **MHC-I is a predominant target of anti-DFT antibody responses**

422   It was previously reported that the antibodies from devils infected with DFT1 were specific to

423   MHC-I, as determined by incubating serum from these devils with IFNG-treated DFT cells[12].

424   Considering the diverse roles of IFNG, there could be other IFNG-induced antigens that can

425   serve as targets for the anti-DFT antibody response.

426

427   To establish if MHC-I is the target of anti-DFT serum antibodies, surface MHC-I expression

428   was first ablated by knocking out the hemizygous *B2M* allele[10] in wild-type DFT1 cells

429   (DFT1.WT) and NLRC5-overexpressing DFT1 cells (DFT1.NLRC5) using CRISPR/Cas9

430   technology. Gene disruption of *B2M* was confirmed by genomic DNA sequencing

431   (**Supplementary Fig. 2**), and flow cytometry using a monoclonal anti-B2M antibody (**Fig. 7**).

432   CRISPR/Cas9-mediated *B2M* knockout (B2M$^{-/-}$) in DFT1 cells rendered the cells irreversibly

433   deficient for surface expression of B2M despite IFNG and NLRC5 stimulation (DFT1.B2M$^{-/-}$

434   + IFNG and DFT1.NLRC5.B2M$^{-/-}$). Due to the pivotal role of B2M in stability of MHC-I

435   complex formation and surface presentation[58–62], absence of surface B2M is indicative of a lack

436   of surface MHC-I expression.

437

438   After surface MHC-I ablation was confirmed, serum from six wild devils (TD1–TD6) that

439   demonstrated anti-DFT responses including natural DFT1 regressions[12] was tested against

440   *B2M* knockout cell lines DFT1.B2M$^{-/-}$ and DFT1.NLRC5.B2M$^{-/-}$. Serum from a healthy devil

441   (TD7) and an immunized devil with induced tumor regression (My)[48] were used as negative

442   and positive controls for antibody binding. All six sera from DFTD$^+$ devils (TD1–TD6) showed

443   weak to no binding to DFT1.WT and DFT1.BFP, which are inherently negative for surface

444   MHC-I (**Fig. 7**). With forced expression of MHC-I using IFNG (DFT1.WT + IFNG) and

445   NLRC5 (DFT1.NLRC5), a positive shift in antibody binding was observed. There was no

446   apparent difference in the level of antibody binding between IFNG-treated and NLRC5-

447   overexpressing DFT1 cells, suggesting a similarity between the antibody target(s) induced by

448   IFNG and NLRC5. Following *B2M* knockout, antibody binding of all six sera was reduced in

449   both IFNG-induced (DFT1.B2M$^{-/-}$ + IFNG) and NLRC5-induced *B2M* knockout DFT1 cells

450   (DFT1.NLRC5.B2M$^{-/-}$), suggesting that MHC-I is a target of DFT1-specific antibody

451   responses in natural tumor regressions.

14

452

DISCUSSION

454 Overexpression of NLRC5 in DFT cells has revealed a major and evolutionarily conserved role

455 for NLRC5 in MHC-I antigen processing and presentation. Consistent with studies in human

456 and mouse cell lines[9,18,63–65], NLRC5 induced expression of classical MHC-I genes (*SAHAI-*

457 *01, SAHAI (LOC105750614), SAHAI (LOC100927947)), B2M, PSMB8, PSMB9* and *TAP1* in

458 both DFT1 and DFT2 cells. Despite the lack of increase in *TAP2* expression, the selective

459 upregulation of MHC-I and other functionally-related genes by NLRC5 was sufficient to

460 restore MHC-I molecules on the cell surface. Although the peptide transport function of TAP

461 proteins typically involves the formation of TAP1 and TAP2 heterodimers, homodimerization

462 of TAP proteins have been described[66,67]. However, the functionality of TAP1 homodimers

463 remains to be verified. The conservation of genes of the MHC-I pathway, regulated by NLRC5

464 across species, highlights the important role of NLRC5 in MHC-I regulation.

465

466 Previous studies have shown that sera from wild devils with anti-DFT immune responses

467 contained high titers of antibody that bound to IFNG-treated DFT1 cells. It was proposed that

468 the primary antibody targets were MHC-I proteins[12]. Additionally, some of these devils

469 experienced tumor regression despite the lack of strong evidence for immune cell infiltration

470 into tumors. The function of NLRC5 that is mainly restricted to MHC-I regulation compared

471 with IFNG provided an opportunity to re-examine antibody target(s) of serum antibodies from

472 wild devils burdened with DFTs. A clear understanding of immunogenic targets of DFTs will

473 provide direction for a more effective vaccine against DFTs.

474

475 The MHC-I complex was identified as the predominant target of anti-DFT serum antibodies.

476 The antibody binding intensity against NLRC5-overexpressing DFT cells was similar to IFNG-

477 treated DFT cells, suggesting similar levels of target antigen expression. When MHC-I

478 expression was ablated through *B2M* knockout, antibody binding was reduced to almost

479 background levels despite IFNG and NLRC5 stimulation. This discovery presents an option to

480 exploit NLRC5 for induction of anti-DFT immunity via MHC-I expression, potentiated by the

481 humoral anti-tumor response in Tasmanian devils. Although cellular immunity is likely a key

482 mechanism for tumor rejection, B cells and antibodies can play eminent roles in transplant

483 rejection[68] and anti-tumor immunity[69]. B cells can promote rejection through antibody-

484 dependent mechanisms that facilitate FcR-mediated phagocytosis by macrophages, antibody-

485 dependent cellular cytotoxicity (ADCC) by NK cells, complement activation and antigen

15

486   uptake by dendritic cells (reviewed by Yuen et al.)[70]. Moreover, B cells can enhance immune

487   surveillance and response through direct antigen presentation to T cells and production of

488   immune-modulating molecules such as cytokines and chemokines[70].

489

490   Caldwell et al. reported that the most highly expressed MHC alleles on DFT2 cells are those

491   that matched host MHC alleles[14], which suggests that DFT cells may hide from host defenses

492   or induce immunological tolerance via shared MHC alleles. If MHC-I is the major antibody

493   target and potentially the overall immune system target, devils having the largest MHC

494   mismatch with DFT cells will be the most likely to have strong MHC-I specific responses and

495   reject DFTs, leading to natural selection in the wild. For example, previous studies have shown

496   that some devils have no functional MHC-I allele at the UA loci and that these individuals can

497   be homozygous at the UB and UC loci[48]. These individuals present a reduced MHC-peptide

498   that would have the lowest probability of a match to the DFT MHC alleles that induce host

499   DFT1 tolerance. However, selection for reduced genetic diversity in MHC alleles would be

500   unfavorable for long-term conservation. A prophylactic vaccine would ideally be designed to

501   assist in the preservation of the genetic diversity of wild devils[71].

502

503   Although the MHC proteins themselves are likely a primary target of humoral and cellular

504   immunity, MHC-I alleles generally differ by only a few amino acids[14,72]. Mutations in DFTs

505   and somatic variation between host and tumor cells provide a rich source of additional antigenic

506   targets for humoral and cellular immunity[10]. The reduction in antibody binding to *B2M*

507   knockout cells suggests that these tumor antigens are unlikely to be the primary antibody

508   targets, although binding of antibodies to peptide-MHC complexes cannot be excluded.

509   Knocking out individual MHC alleles in DFT cells or overexpression of MHC alleles in

510   alternative non-DFT cell lines could be used to disentangle the importance of specific alleles

511   and investigate the potential for peptide-MHC complexes to be antibody targets.

512

513   Our results confirm that IFNG affects more immunoregulatory processes than NLRC5.

514   However, the functional dichotomy of IFNG in cancer means that NLRC5 modulation could

515   be an alternative to IFNG treatment for enhancing tumor cell immunogenicity in a range of

516   species, including human. Importantly, NLRC5 upregulated B2M on the surface of DFT cells

517   to similar levels as IFNG, but it does not upregulate inhibitory molecules. The restoration of

518   functional MHC-I molecules without concomitant upregulation of PDL1 and SAHA-UK has

519   multiple advantages over IFNG for triggering effective cytotoxic responses against DFT cells.

16

520   First, cells transfected with NLRC5 constitutively express MHC-I and therefore do not require

521   culturing in IFNG, which can be problematic as IFNG can also reduce cell viability[17]. Second,

522   PDL1 negatively regulates T cell responses by inducing T cell anergy[73] and apoptosis[74] while

523   limiting T cell activity[75]. Moreover, PDL1 promotes tumor growth and survival by stimulating

524   cell proliferation[76] and resistance to T cell killing[77,78]. Third, the expression of monomorphic

525   MHC-I SAHA-UK induced by IFNG would allow DFT cells to escape cytotoxic attack from

526   both NK cells and CD8^{+} T cells[79]. Fourth, several other immune checkpoint protein receptor-

527   ligand interactions were recently shown to be conserved in devils[80,81], but we found no

528   significant upregulation of these genes by NLRC5. The ability to improve tumor

529   immunogenicity in the absence of inhibitory signals has positive implications for immunization

530   and immunotherapeutic strategies. NLRC5 could evoke protective anti-tumor immunity

531   against DFTs, similar to NLRC5-expressing B16-F10 melanoma cells in mice[64].

532

533   The absence of a regulatory effect on *SAHA-UK* and *PDL1* by NLRC5 in contrast to IFNG

534   could be due to the composition of the promoter elements of these genes. The promoter of

535   MHC class I genes consists of three conserved cis-regulatory elements: a NFκB-binding

536   Enhancer A region, an interferon-stimulated response element (ISRE) and a SXY module[82,83].

537   The SXY module is critical for NLRC5-mediated MHC-I transactivation as it serves as the

538   binding site for the multi-protein complex formed between NLRC5 and various transcription

539   factors[19,21,84]. An ISRE and SXY module is present within 200 base pairs of the start codon for

540   all three classical devil MHC-I genes[51]. We identified an ISRE element in the *SAHA-UK*

541   promoter region but were unable to identify an SXY module in this region. This could explain

542   the upregulation of *SAHA-UK* upon IFNG stimulation but not in NLRC5-overexpressing DFT

543   cells. Similarly, the SXY module was not identified in orthologues of *SAHA-UK,* which are

544   *Modo-UK* in the grey short-tailed opossum[85] and *Maeu-UK* in the tammar wallaby[86]. The

545   difference in regulation and therefore, pattern of expression of the UK gene in marsupials[85–87]

546   may reflect a separate function from classical MHC-I. The marsupial UK gene has been

547   hypothesized to play a marsupial-specific role in conferring immune protection to vulnerable

548   newborn marsupials during their pouch life[86]. SXY modules are typically not found in the

549   promoter region of PDL1[88] therefore, it is not expected for NLRC5 to be a regulator of PDL1.

550   Rather, IFNG-mediated induction of PDL1 occurs via transcription factor interferon regulatory

551   factor 1 (IRF-1)[88], which is induced by STAT1[89].

552

553   Beyond MHC-I regulation, NLRC5 expression in DFT1 cells displayed other beneficial

554   immune-regulating functions, mainly via the non-canonical β-catenin-independent WNT

555   signaling pathway. One of the downstream effectors that was upregulated by NLRC5 included

556   *PRKCB*, an activator of NFκB in B cells[90]. NFκB is a family of pleiotropic transcription factors

557   known to regulate several immune and inflammatory responses including cellular processes

558   such as cell proliferation and apoptosis[91]. In recent years, aberrations in NFκB signaling have

559   been implicated in cancer development and progression[92,93]. The regulation of NFκB signaling

560   by NLRC5 has been documented in several studies although the findings have been

561   contradictory[54,55,94,95].

562

563   In summary, we have demonstrated the role of NLRC5 in MHC-I regulation of DFT cells

564   thereby, displaying the functional conservation of NLRC5 across species. The finding that

565   MHC-I is a major antibody target in wild devils with anti-DFT response and natural DFT

566   regression can help guide DFTD vaccine development and conservation management

567   strategies. NLRC5-overexpressing DFT cells can be harnessed to elicit both cellular and

568   humoral immunity against future and pre-existing DFT infections in wild devils using MHC-I

569   as a target. Given the prevalence of altered MHC-I expression in cancer as a form of immune

570   escape mechanism[96–98], NLRC5 presents as a new target for providing an insight into the role

571   of MHC-I in cancer as well as transplantation, and its manipulation for human cancer treatment

572   and transplant tolerance.

573

584

585   **AUTHOR CONTRIBUTIONS**

586   ABL, ALP, ASF, CEBO and GMW designed the study. ALP, ASF, CEBO, GSL, JC, and JMD

587   developed the technology. CEBO and JMD performed the experiments. ALP and CEBO

588   performed bioinformatic analyses. CEBO created the figures. ALP, ASF, and CEBO analyzed

589   the data. CEBO wrote the manuscript, and all authors edited the manuscript.

590

591   **CONFLICT OF INTEREST**

592   The authors declare that the research was conducted in the absence of any commercial or

593   financial relationships that could be construed as a potential conflict of interest.

REFERENCES

1   Jones ME, Paetkau D, Geffen E, Moritz C. Genetic diversity and population structure of Tasmanian devils, the largest marsupial carnivore. *Mol Ecol* 2004; **13**: 2197–2209.

2   Loh R, Hayes D, Mahjoor A, O'Hara A, Pyecroft S, Raidal S. The Immunohistochemical Characterization of Devil Facial Tumor Disease (DFTD) in the Tasmanian Devil (Sarcophilus harrisii). *Vet Pathol* 2006; **43**: 896–903.

3   Pearse A-M, Swift K. Allograft theory: Transmission of devil facial-tumour disease. *Nature* 2006; **439**: 549.

4   Pye RJ, Pemberton D, Tovar C, Tubio JMC, Dun KA, Fox S *et al.* A second transmissible cancer in Tasmanian devils. *Proc Natl Acad Sci U S A* 2016; **113**: 374–379.

5   Murchison EP, Tovar C, Hsu A, Bender HS, Kheradpour P, Rebbeck CA *et al.* The Tasmanian devil transcriptome reveals Schwann cell origins of a clonally transmissible cancer. *Science* 2010; **327**: 84–87.

6   Patchett AL, Coorens THH, Darby J, Wilson R, McKay MJ, Kamath KS *et al.* Two of a kind: transmissible Schwann cell cancers in the endangered Tasmanian devil (*Sarcophilus harrisii*). *Cell Mol Life Sci* 2020; **77**: 1847–1858.

7   Lazenby BT, Tobler MW, Brown WE, Hawkins CE, Hocking GJ, Hume F *et al.* Density trends and demographic signals uncover the long-term impact of transmissible cancer in Tasmanian devils. *J Appl Ecol* 2018; **55**: 1368–1379.

8   Siddle H V, Kreiss A, Tovar C, Yuen CK, Cheng Y, Belov K *et al.* Reversible epigenetic down-regulation of MHC molecules by devil facial tumour disease illustrates immune escape by a contagious cancer. *Proc Natl Acad Sci U S A* 2013; **110**: 5103–5108.

9   Yoshihama S, Roszik J, Downs I, Meissner TB, Vijayan S, Chapuy B *et al.* NLRC5/MHC class I transactivator is a target for immune evasion in cancer. *Proc Natl Acad Sci U S A* 2016; **113**: 5999–6004.

10   Stammnitz MR, Coorens THH, Gori KC, Hayes D, Fu B, Wang J *et al.* The Origins and Vulnerabilities of Two Transmissible Cancers in Tasmanian Devils. *Cancer Cell* 2018; **33**: 607-619.e15.

11   Brown GK, Kreiss A, Lyons AB, Woods GM. Natural killer cell mediated cytotoxic responses in the Tasmanian devil. *PLoS One* 2011; **6**: e24475.

12   Pye R, Hamede R, Siddle H V., Caldwell A, Knowles GW, Swift K *et al.* Demonstration of immune responses against devil facial tumour disease in wild

20

628   Tasmanian devils. *Biol Lett* 2016; **12**: 20160553.

629   13   Pye R, Patchett A, McLennan E, Thomson R, Carver S, Fox S *et al.* Immunization

630   Strategies Producing a Humoral IgG Immune Response against Devil Facial Tumor

631   Disease in the Majority of Tasmanian Devils Destined for Wild Release. *Front*

632   *Immunol* 2018; **9**: 259.

633   14   Caldwell A, Coleby R, Tovar C, Stammnitz MR, Kwon YM, Owen RS *et al.* The

634   newly-arisen Devil facial tumour disease 2 (DFT2) reveals a mechanism for the

635   emergence of a contagious cancer. *Elife* 2018; **7**: e35314.

636   15   Zaidi MR. The Interferon-Gamma Paradox in Cancer. *J Interf Cytokine Res* 2019; **39**:

637   30–38.

638   16   Flies AS, Lyons AB, Corcoran LM, Papenfuss AT, Murphy JM, Knowles GW *et al.*

639   PD-L1 is not constitutively expressed on Tasmanian devil facial tumor cells but is

640   strongly upregulated in response to IFN-γ and can be expressed in the tumor

641   microenvironment. *Front Immunol* 2016; **7**: 581.

642   17   Ong CEB, Lyons AB, Woods GM, Flies AS. Inducible IFN-γ Expression for MHC-I

643   Upregulation in Devil Facial Tumor Cells. *Front Immunol* 2019; **9**: 3117.

644   18   Meissner TB, Li A, Biswas A, Lee K-H, Liu Y-J, Bayir E *et al.* NLR family member

645   NLRC5 is a transcriptional regulator of MHC class I genes. *Proc Natl Acad Sci U S A*

646   2010; **107**: 13794–13799.

647   19   Meissner TB, Liu Y-J, Lee K-H, Li A, Biswas A, van Eggermond MCJA *et al.*

648   NLRC5 cooperates with the RFX transcription factor complex to induce MHC class I

649   gene expression. *J Immunol* 2012; **188**: 4951–4958.

650   20   Gobin SJP, van Zutphen M, Westerheide SD, Boss JM, van den Elsen PJ. The MHC-

651   specific enhanceosome and its role in MHC class I and β2-microglobulin gene

652   transactivation. *J Immunol* 2001; **167**: 5175–5184.

653   21   Neerincx A, Rodriguez GM, Steimle V, Kufer TA. NLRC5 controls basal MHC class I

654   gene expression in an MHC enhanceosome-dependent manner. *J Immunol* 2012; **188**:

655   4940–4950.

656   22   Benkő S, Kovács EG, Hezel F, Kufer TA. NLRC5 Functions beyond MHC I

657   Regulation-What Do We Know So Far? *Front Immunol* 2017; **8**: 150.

658   23   Pearse A-M, Swift K, Hodson P, Hua B, McCallum H, Pyecroft S *et al.* Evolution in a

659   transmissible cancer: a study of the chromosomal changes in devil facial tumor (DFT)

660   as it spreads through the wild Tasmanian devil population. *Cancer Genet* 2012; **205**:

661   101–112.

662 24 Patchett AL, Wilson R, Charlesworth JC, Corcoran LM, Papenfuss AT, Lyons BA *et*
663 *al.* Transcriptome and proteome profiling reveals stress-induced expression signatures
664 of imiquimod-treated Tasmanian devil facial tumor disease (DFTD) cells. *Oncotarget*
665 2018; **9**: 15895–15914.

666 25 Andrews S. FastQC: A Quality Control tool for High Throughput Sequence Data.
667 2010.https://www.bioinformatics.babraham.ac.uk/projects/fastqc/.

668 26 Liao Y, Smyth GK, Shi W. The Subread aligner: fast, accurate and scalable read
669 mapping by seed-and-vote. *Nucleic Acids Res* 2013; **41**: e108–e108.

670 27 Liao Y, Smyth GK, Shi W. featureCounts: an efficient general purpose program for
671 assigning sequence reads to genomic features. *Bioinformatics* 2014; **30**: 923–930.

672 28 RStudio Team. RStudio: Integrated Development Environment for R.
673 2020.http://www.rstudio.com/.

674 29 R Core Team. R: A Language and Environment for Statistical Computing.
675 2020.https://www.r-project.org/.

676 30 Robinson MD, McCarthy DJ, Smyth GK. edgeR: A Bioconductor package for
677 differential expression analysis of digital gene expression data. *Bioinformatics* 2009;
678 **26**: 139–140.

679 31 Robinson MD, Oshlack A. A scaling normalization method for differential expression
680 analysis of RNA-seq data. *Genome Biol* 2010; **11**: R25.

681 32 Anders S, Huber W. Differential expression analysis for sequence count data. *Genome*
682 *Biol* 2010; **11**: R106.

683 33 Bullard JH, Purdom E, Hansen KD, Dudoit S. Evaluation of statistical methods for
684 normalization and differential expression in mRNA-Seq experiments. *BMC*
685 *Bioinformatics* 2010; **11**: 94.

686 34 Risso D, Schwartz K, Sherlock G, Dudoit S. GC-Content Normalization for RNA-Seq
687 Data. *BMC Bioinformatics* 2011; **12**: 480.

688 35 Law CW, Chen Y, Shi W, Smyth GK. voom: Precision weights unlock linear model
689 analysis tools for RNA-seq read counts. *Genome Biol* 2014; **15**: R29.

690 36 Ritchie ME, Phipson B, Wu D, Hu Y, Law CW, Shi W *et al. limma* powers differential
691 expression analyses for RNA-sequencing and microarray studies. *Nucleic Acids Res*
692 2015; **43**: e47.

693 37 Phipson B, Lee S, Majewski IJ, Alexander WS, Smyth GK. Robust hyperparameter
694 estimation protects against hypervariable genes and improves power to detect
695 differential expression. *Ann Appl Stat* 2016; **10**: 946–963.

696   38   Oliveros JC. Venny. An interactive tool for comparing lists with Venn's diagrams.

697   2015.https://bioinfogp.cnb.csic.es/tools/venny/index.html.

698   39   Gu Z, Eils R, Schlesner M. Complex heatmaps reveal patterns and correlations in

699   multidimensional genomic data. *Bioinformatics* 2016; **32**: 2847–2849.

700   40   Yu G, Wang LG, Han Y, He QY. ClusterProfiler: An R package for comparing

701   biological themes among gene clusters. *Omi A J Integr Biol* 2012; **16**: 284–287.

702   41   Yu G, He QY. ReactomePA: An R/Bioconductor package for reactome pathway

703   analysis and visualization. *Mol Biosyst* 2016; **12**: 477–479.

704   42   Kowarz E, Löscher D, Marschalek R. Optimized Sleeping Beauty transposons rapidly

705   generate stable transgenic cell lines. *Biotechnol J* 2015; **10**: 647–653.

706   43   Flies AS, Darby JM, Murphy PR, Pinfold TL, Patchett AL, Lennard PR. Generation

707   and Testing of Fluorescent Adaptable Simple Theranostic (FAST) Proteins. *Bio-*

708   *protocol* 2020; **10**: e3696.

709   44   Mátés L, Chuah MKL, Belay E, Jerchow B, Manoj N, Acosta-Sanchez A *et al.*

710   Molecular evolution of a novel hyperactive Sleeping Beauty transposase enables

711   robust stable gene transfer in vertebrates. *Nat Genet* 2009; **41**: 753–761.

712   45   Labun K, Montague TG, Krause M, Torres Cleuren YN, Tjeldnes H, Valen E.

713   CHOPCHOP v3: Expanding the CRISPR web toolbox beyond genome editing.

714   *Nucleic Acids Res* 2019; **47**: W171–W174.

715   46   Sanjana NE, Shalem O, Zhang F. Improved vectors and genome-wide libraries for

716   CRISPR screening. *Nat Methods* 2014; **11**: 783–784.

717   47   Synthego. Synthego Performance Analysis, ICE Analysis.

718   2019.https://www.synthego.com/products/bioinformatics/crispr-analysis (accessed 31

719   Jul2020).

720   48   Tovar C, Pye RJ, Kreiss A, Cheng Y, Brown GK, Darby J *et al.* Regression of devil

721   facial tumour disease following immunotherapy in immunised Tasmanian devils. *Sci*

722   *Rep* 2017; **7**: 43827.

723   49   Howson LJ, Morris KM, Kobayashi T, Tovar C, Kreiss A, Papenfuss AT *et al.*

724   Identification of dendritic cells, B cell and T cell subsets in Tasmanian devil lymphoid

725   tissue; evidence for poor immune cell infiltration into devil facial tumors. *Anat Rec*

726   *(Hoboken)* 2014; **297**: 925–938.

727   50   Tovar C, Obendorf D, Murchison EP, Papenfuss AT, Kreiss A, Woods GM. Tumor-

728   specific diagnostic marker for transmissible facial tumors of Tasmanian devils:

729   immunohistochemistry studies. *Vet Pathol* 2011; **48**: 1195–1203.

730   51   Cheng Y, Stuart A, Morris K, Taylor R, Siddle H, Deakin J *et al.* Antigen-presenting
731   genes and genomic copy number variations in the Tasmanian devil MHC. *BMC*
732   *Genomics* 2012; **13**: 87.

733   52   Kuenzel S, Till A, Winkler M, Häsler R, Lipinski S, Jung S *et al.* The nucleotide-
734   binding oligomerization domain-like receptor NLRC5 is involved in IFN-dependent
735   antiviral immune responses. *J Immunol* 2010; **184**: 1990–2000.

736   53   Neerincx A, Lautz K, Menning M, Kremmer E, Zigrino P, Hösel M *et al.* A role for
737   the human nucleotide-binding domain, leucine-rich repeat-containing family member
738   NLRC5 in antiviral responses. *J Biol Chem* 2010; **285**: 26223–26232.

739   54   Cui J, Zhu L, Xia X, Wang HY, Legras X, Hong J *et al.* NLRC5 negatively regulates
740   the NF-kappaB and type I interferon signaling pathways. *Cell* 2010; **141**: 483–496.

741   55   Benko S, Magalhaes JG, Philpott DJ, Girardin SE. NLRC5 Limits the Activation of
742   Inflammatory Pathways. *J Immunol* 2010; **185**: 1681–1691.

743   56   Davis BK, Roberts RA, Huang MT, Willingham SB, Conti BJ, Brickey WJ *et al.*
744   Cutting edge: NLRC5-dependent activation of the inflammasome. *J Immunol* 2011;
745   **186**: 1333–1337.

746   57   Wang J quan, Liu Y ru, Xia Q, Chen R nan, Liang J, Xia Q rong *et al.* Emerging roles
747   for NLRC5 in immune diseases. Front. Pharmacol. 2019; **10**: 1352.

748   58   Boyd LF, Kozlowski S, Margulies DH. Solution binding of an antigenic peptide to a
749   major histocompatibility complex class I molecule and the role of β_2-microglobulin.
750   *Proc Natl Acad Sci U S A* 1992; **89**: 2242–2246.

751   59   Kozlowski S, Takeshita T, Boehncke WH, Takahashi H, Boyd LF, Germain RN *et al.*
752   Excess β_2 microglobulin promoting functional peptide association with purified
753   soluble class I MHC molecules. *Nature* 1991; **349**: 74–77.

754   60   Vitiello A, Potter TA, Sherman LA. The role of beta 2-microglobulin in peptide
755   binding by class I molecules. *Science (80-)* 1990; **250**: 1423–1426.

756   61   Williams DB, Barber BH, Flavell RA, Allen H. Role of beta 2-microglobulin in the
757   intracellular transport and surface expression of murine class I histocompatibility
758   molecules.[erratum appears in J Immunol 1989 Jul 15;143(2):761]. *J Immunol* 1989;
759   **142**: 2796–2806.

760   62   Arce-Gomez B, Jones EA, Barnstable CJ, Solomon E, Bodmer WF. The Genetic
761   Control of HLA-A and B Antigens in Somatic Cell Hybrids: Requirement for β_2
762   Microglobulin. *Tissue Antigens* 1978; **11**: 96–112.

763   63   Biswas A, Meissner TB, Kawai T, Kobayashi KS. Cutting edge: impaired MHC class I

764   expression in mice deficient for NLRC5/class I transactivator. *J Immunol* 2012; **189**:

765   516–520.

766   64   Rodriguez GM, Bobbala D, Serrano D, Mayhue M, Champagne A, Saucier C *et al.*

767   NLRC5 elicits antitumor immunity by enhancing processing and presentation of tumor

768   antigens to CD8^{+} T lymphocytes. *Oncoimmunology* 2016; **5**: e1151593.

769   65   Yao Y, Wang Y, Chen F, Huang Y, Zhu S, Leng Q *et al.* NLRC5 regulates MHC class

770   I antigen presentation in host defense against intracellular pathogens. *Cell Res* 2012;

771   **22**: 836–847.

772   66   Lapinski PE, Miller GG, Tampé R, Raghavan M. Pairing of the nucleotide binding

773   domains of the transporter associated with antigen processing. *J Biol Chem* 2000; **275**:

774   6831–6840.

775   67   Antoniou AN, Ford S, Pilley ES, Blake N, Powis SJ. Interactions formed by

776   individually expressed TAP1 and TAP2 polypeptide subunits. *Immunology* 2002; **106**:

777   182–189.

778   68   Schmitz R, Fitch ZW, Schroder PM, Choi AY, Jackson AM, Knechtle SJ *et al.* B cells

779   in transplant tolerance and rejection: friends or foes? *Transpl Int* 2020; **33**: 30–40.

780   69   Nelson BH. CD20 + B Cells: The Other Tumor-Infiltrating Lymphocytes . *J Immunol*

781   2010; **185**: 4977–4982.

782   70   Yuen GJ, Demissie E, Pillai S. B Lymphocytes and Cancer: A Love–Hate

783   Relationship. *Trends in Cancer* 2016; **2**: 747–757.

784   71   Flies AS, Flies EJ, Fox S, Gilbert A, Johnson SR, Liu G-S *et al.* An oral bait

785   vaccination approach for the Tasmanian devil facial tumor diseases. *Expert Rev*

786   *Vaccines* 2020; **19**: 1–10.

787   72   Gastaldello A, Sh R, Bailey A, Owen R, Turner S, Kontouli A *et al.* Passage of

788   transmissible cancers in the Tasmanian devil is due to a dominant, shared peptide

789   motif and a limited repertoire of MHC-I allotypes. *bioRxiv* 2020.

790   doi:10.1101/2020.07.03.184416.

791   73   Selenko-Gebauer N, Majdic O, Szekeres A, Höfler G, Guthann E, Korthäuer U *et al.*

792   B7-H1 (Programmed Death-1 Ligand) on Dendritic Cells Is Involved in the Induction

793   and Maintenance of T Cell Anergy. *J Immunol* 2003; **170**: 3637–3644.

794   74   Dong H, Strome SE, Salomao DR, Tamura H, Hirano F, Flies DB *et al.* Tumor-

795   associated B7-H1 promotes T-cell apoptosis: A potential mechanism of immune

796   evasion. *Nat Med* 2002; **8**: 793–800.

797   75   Butte MJ, Keir ME, Phamduy TB, Sharpe AH, Freeman GJ. Programmed death-1

798   ligand 1 interacts specifically with the B7-1 costimulatory molecule to inhibit T cell

799   responses. *Immunity* 2007; **27**: 111–122.

800   76   Ghebeh H, Tulbah A, Mohammed S, ElKum N, Amer SM Bin, Al-Tweigeri T *et al.*

801   Expression of B7-H1 in breast cancer patients is strongly associated with high

802   proliferative Ki-67-expressing tumor cells. *Int J Cancer* 2007; **121**: 751–758.

803   77   Iwai Y, Ishida M, Tanaka Y, Okazaki T, Honjo T, Minato N. Involvement of PD-L1

804   on tumor cells in the escape from host immune system and tumor immunotherapy by

805   PD-L1 blockade. *Proc Natl Acad Sci U S A* 2002; **99**: 12293–12297.

806   78   Azuma T, Yao S, Zhu G, Flies AS, Flies SJ, Chen L. B7-H1 is a ubiquitous

807   antiapoptotic receptor on cancer cells. *Blood* 2008; **111**: 3635–3643.

808   79   Kochan G, Escors D, Breckpot K, Guerrero-Setas D. Role of non-classical MHC class

809   I molecules in cancer immunosuppression. Oncoimmunology. 2013; **2**: e26491.

810   80   Flies AS, Blackburn NB, Lyons AB, Hayball JD, Woods GM. Comparative Analysis

811   of Immune Checkpoint Molecules and Their Potential Role in the Transmissible

812   Tasmanian Devil Facial Tumor Disease. *Front Immunol* 2017; **8**: 513.

813   81   Flies AS, Darby JM, Lennard PR, Murphy PR, Ong CEB, Pinfold TL *et al.* A novel

814   system to map protein interactions reveals evolutionarily conserved immune evasion

815   pathways on transmissible cancers. *Sci Adv* 2020; **6**: eaba5031.

816   82   Van Den Elsen PJ, Gobin SJP, Van Eggermond MCJA, Peijnenburg A. Regulation of

817   MHC class I and II gene transcription: Differences and similarities. *Immunogenetics*

818   1998; **48**: 208–221.

819   83   Van Den Elsen PJ, Peijnenburg A, Van Eggermond MC j. a., Gobin SJ p. Shared

820   regulatory elements in the promoters of MHC class I and class II genes. *Immunol*

821   *Today* 1998; **19**: 308–312.

822   84   Ludigs K, Seguín-Estévez Q, Lemeille S, Ferrero I, Rota G, Chelbi S *et al.* NLRC5

823   exclusively transactivates MHC class I and related genes through a distinctive SXY

824   module. *PLoS Genet* 2015; **11**: e1005088.

825   85   Belov K, Deakin JE, Papenfuss AT, Baker ML, Melman SD, Siddle H V *et al.*

826   Reconstructing an Ancestral Mammalian Immune Supercomplex from a Marsupial

827   Major Histocompatibility Complex. *PLoS Biol* 2006; **4**: e46.

828   86   Siddle H V., Deakin JE, Coggill P, Hart E, Cheng Y, Wong ESW *et al.* MHC-linked

829   and un-linked class I genes in the wallaby. *BMC Genomics* 2009; **10**: 310.

830   87   Cheng Y, Belov K. Characterisation of non-classical MHC class I genes in the

831   Tasmanian devil (*Sarcophilus harrisii*). *Immunogenetics* 2014; **66**: 727–735.

832 88 Lee S-J, Jang B-C, Lee S-W, Yang Y-I, Suh S-I, Park Y-M *et al.* Interferon regulatory
833   factor-1 is prerequisite to the constitutive expression and IFN-γ-induced upregulation
834   of B7-H1 (CD274). *FEBS Lett* 2006; **580**: 755–762.

835 89 Loke P, Allison JP. PD-L1 and PD-L2 are differentially regulated by Th1 and Th2
836   cells. *Proc Natl Acad Sci USA* 2003; **100**: 5336–5341.

837 90 Saijo K, Mecklenbräuker I, Santana A, Leitger M, Schmedt C, Tarakhovsky A. Protein
838   kinase C β controls nuclear factor κB activation in B cells through selective regulation
839   of the IκB kinase α. *J Exp Med* 2002; **195**: 1647–1652.

840 91 Hayden MS, Ghosh S. Signaling to NF-κB. *Genes Dev* 2004; **18**: 2195–2224.

841 92 Xia L, Tan S, Zhou Y, Lin J, Wang H, Oyang L *et al.* Role of the NFκB-signaling
842   pathway in cancer. *Onco Targets Ther* 2018; **11**: 2063–2073.

843 93 Verzella D, Pescatore A, Capece D, Vecchiotti D, Ursini MV, Franzoso G *et al.* Life,
844   death, and autophagy in cancer: NF-κB turns up everywhere. *Cell Death Dis* 2020; **11**:
845   1–14.

846 94 Tong Y, Cui J, Li Q, Zou J, Wang HY, Wang R-F. Enhanced TLR-induced NF-κB
847   signaling and type I interferon responses in NLRC5 deficient mice. *Cell Res* 2012; **22**:
848   822–35.

849 95 Liu Y ru, Yan X, Yu H xia, Yao Y, Wang J quan, Li X feng *et al.* NLRC5 promotes
850   cell proliferation via regulating the NF-κB signaling pathway in Rheumatoid arthritis.
851   *Mol Immunol* 2017; **91**: 24–34.

852 96 Garrido F, Cabrera T, Concha A, Glew S, Ruiz-Cabello F, Stern PL. Natural history of
853   HLA expression during tumour development. Immunol. Today. 1993; **14**: 491–499.

854 97 Hicklin DJ, Marincola FM, Ferrone S. HLA class I antigen downregulation in human
855   cancers: T-cell immunotherapy revives an old story. Mol. Med. Today. 1999; **5**: 178–
856   186.

857 98 Campoli M, Ferrone S. HLA antigen changes in malignant cells: Epigenetic
858   mechanisms and biologic significance. Oncogene. 2008; **27**: 5869–5885.

859 **TABLES**

860 **Table 1.** Devil facial tumor (DFT) cell lines and treatments

ID #	Sample name	Parent cell line	Treatment
1	DFT1.WT*	DFT1 C5065	Untreated
2	DFT1.WT + IFNG	DFT1 C5065	5 ng/mL IFNG, 24h
3	DFT2.WT^{RV}*	DFT2 RV	Untreated
4	DFT2.WT^{RV} + IFNG	DFT2 RV	5 ng/mL IFNG, 24h
5	DFT1.BFP	DFT1 C5065	Transfected with control vector pSBbi-BH
6	DFT1.NLRC5	DFT1 C5065	Transfected with NLRC5 vector pCO1
7	DFT2.WT	DFT2 JV	Untreated
8	DFT2.BFP	DFT2 JV	Transfected with control vector pSBbi-BH
9	DFT2.NLRC5	DFT2 JV	Transfected with NLRC5 vector pCO1
10	DFT1.B2M$^{-/-}$	DFT1 C5065	Transfected with *B2M* targeting vector pAF217
11	DFT1.B2M$^{-/-}$ + IFNG	DFT1 C5065	Transfected with *B2M* targeting vector pAF217 and treated with 5 ng/mL IFNG for 24h
12	DFT1.NLRC5.B2M$^{-/-}$	DFT1 C5065	Transfected with NLRC5 vector pCO1 and *B2M* targeting vector pAF218

861 *DFT1.WT data from Patchett et al., 2018[24] and DFT2.WT^{RV} from Patchett et al., 2020[6] available
862 through European Nucleotide Archive # PRJNA416378 and # PRJEB28680, respectively.

863 **Table 2.** Reactome pathways enriched in differentially expressed genes in DFT1.NLRC5

Reactome ID	Pathway	Count	Term size	p-value	p.adjust	Genes
Upregulated						
R-HSA-1236974	ER-Phagosome pathway	4	74	4.69E-05	4.75E-03	*B2M, PSMB8, PSMB9, TAP1*
R-HSA-1168372	Downstream signaling events of B Cell Receptor (BCR)	4	80	6.37E-05	4.75E-03	*NFATC1, PRKCB, PSMB8, PSMB9*
R-HSA-1236975	Antigen processing-Cross presentation	4	81	6.69E-05	4.75E-03	*B2M, PSMB8, PSMB9, TAP1*
R-HSA-983705	Signaling by the B Cell Receptor (BCR)	4	104	1.77E-04	9.44E-03	*NFATC1, PRKCB, PSMB8, PSMB9*
R-HSA-3858494	Beta-catenin independent WNT signaling	4	129	4.06E-04	1.73E-02	*NFATC1, PRKCB, PSMB8, PSMB9*
R-HSA-1169091	Activation of NF-kappaB in B cells	3	64	7.19E-04	2.55E-02	*PRKCB, PSMB8, PSMB9*
Downregulated						
R-HSA-216083	Integrin cell surface interactions	5	62	1.16E-05	4.04E-03	*CDH1, COL18A1, COL6A1, COL6A2, JAM2*
R-HSA-1251985	Nuclear signaling by ERBB4	3	28	3.33E-04	4.93E-02	*EREG, GFAP, S100B*
R-HSA-5173105	O-linked glycosylation	4	73	4.27E-04	4.93E-02	*ADAMTS7, B3GNT7, GALNT13, GALNT17*
R-HSA-913709	O-linked glycosylation of mucins	3	34	5.96E-04	4.93E-02	*B3GNT7, GALNT13, GALNT17*
R-HSA-8948216	Collagen chain trimerization	3	36	7.06E-04	4.93E-02	*COL18A1, COL6A1, COL6A2*

Cut-offs p-value < 0.001 and p.adjust < 0.05 were used to display significant pathways. P-values were adjusted (p.adjust) for multiple testing using Benjamini–Hochberg method. See also Supplementary Table 9 for full list of Reactome pathways.

864

865 **Table 3.** Reactome pathways enriched in differentially expressed genes in DFT2.NLRC5

| Reactome ID	Pathway	Count	Term size	p-value	p.adjust	Genes
Upregulated						
R-HSA-1236974	ER-Phagosome pathway	4	74	3.43E-06	3.80E-04	*B2M, PSMB8, PSMB9, TAP1*
R-HSA-1236975	Antigen processing-Cross presentation	4	81	4.93E-06	3.80E-04	*B2M, PSMB8, PSMB9, TAP1*
R-HSA-983169	Class I MHC mediated antigen processing & presentation	5	312	5.96E-05	3.06E-03	*B2M, PSMB8, PSMB9, TAP1, TRIM69*
R-HSA-983170	Antigen Presentation: Folding, assembly and peptide loading of class I MHC	2	18	3.31E-04	1.27E-02	*B2M, TAP1*
R-HSA-162909	Host Interactions of HIV factors	3	119	6.91E-04	1.36E-02	*B2M, PSMB8, PSMB9*
Downregulated						
R-HSA-112316	Neuronal System	33	276	1.73E-06	1.28E-03	*see Supplementary Table 10*
R-HSA-1474228	Degradation of the extracellular matrix	16	97	1.82E-05	6.73E-03	*see Supplementary Table 10*
R-HSA-264642	Acetylcholine Neurotransmitter Release Cycle	5	10	5.87E-05	1.45E-02	*see Supplementary Table 10*
R-HSA-181429	Serotonin Neurotransmitter Release Cycle	5	12	1.70E-04	2.27E-02	*see Supplementary Table 10*
R-HSA-181430	Norepinephrine Neurotransmitter Release Cycle	5	12	1.70E-04	2.27E-02	*see Supplementary Table 10*
R-HSA-112315	Transmission across Chemical Synapses	21	179	1.84E-04	2.27E-02	*see Supplementary Table 10*
R-HSA-1474244	Extracellular matrix organization	24	224	2.65E-04	2.80E-02	*see Supplementary Table 10*
R-HSA-166658	Complement cascade	6	21	4.02E-04	3.38E-02	*see Supplementary Table 10*
R-HSA-1296072	Voltage gated Potassium channels	7	29	4.11E-04	3.38E-02	*see Supplementary Table 10*
R-HSA-2022090	Assembly of collagen fibrils and other multimeric structures	9	49	5.62E-04	4.16E-02	*see Supplementary Table 10*
R-HSA-210500	Glutamate Neurotransmitter Release Cycle	5	16	7.96E-04	4.91E-02	*see Supplementary Table 10*
R-HSA-212676	Dopamine Neurotransmitter Release Cycle	5	16	7.96E-04	4.91E-02	*see Supplementary Table 10*

Cut-offs p-value < 0.001 and p.adjust < 0.05 were used to display significant pathways. P-values were adjusted (p.adjust) for multiple testing using Benjamini–Hochberg method. See also Supplementary Table 10 for full list of Reactome pathways.

866

867   **FIGURES**
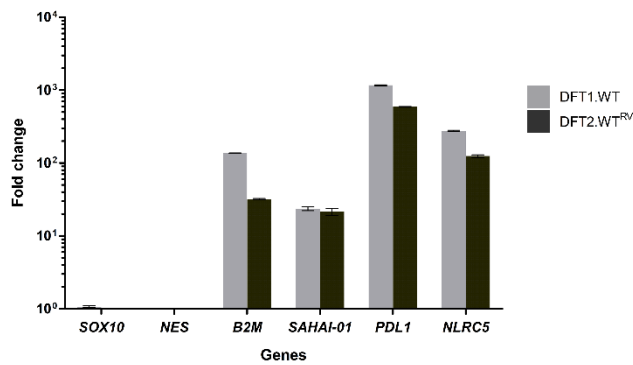
868

869   **Figure 1. Upregulation of NLRC5 by IFNG in DFT1 and DFT2 cells.** Fold change in
870   mRNA expression (transcripts per kilobase million (TPM)) of *B2M*, MHC class I gene *SAHAI-*
871   *01*, *PDL1* and *NLRC5* upon IFNG treatment in DFT1 C5065 cell line (DFT1.WT) and DFT2
872   RV cell line (DFT2.WT^{RV}). *SOX10* and *NES* were included as internal controls. Bars show the
873   mean of *N*=2 replicates per treatment. Error bars indicate standard deviation.

31
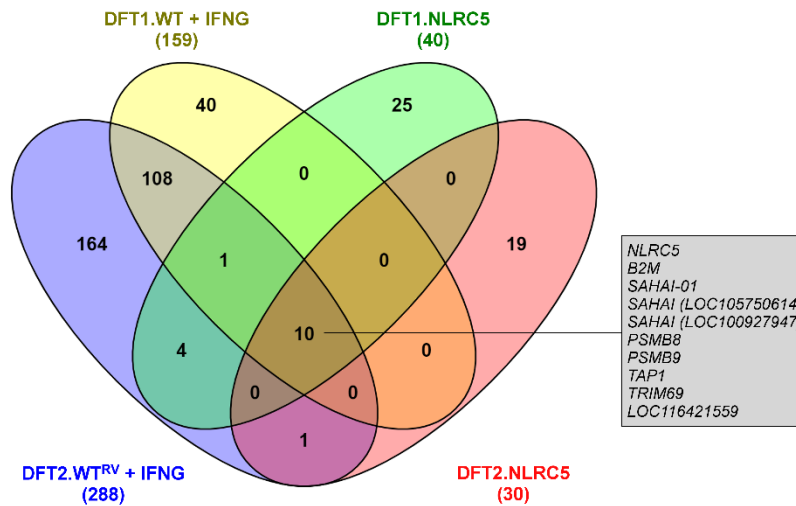
Figure 2. Venn diagram of genes significantly upregulated upon IFNG treatment and NLRC5 overexpression in DFT1 and DFT2 cells. Genes were defined as significantly upregulated when false discovery rate (FDR) < 0.05 and $\log_2 FC \geq 2.0$. Total number of genes upregulated for each treatment is indicated in parentheses under the sample name. The box shows genes upregulated in all four treatments: (i) IFNG-treated DFT1 cells (DFT1.WT + IFNG), (ii) IFNG-treated DFT2 cells (DFT2.WT[RV] + IFNG), (iii) NLRC5-overexpressing DFT1 cells (DFT1.NLRC5), and (iv) NLRC5-overexpressing DFT2 cells (DFT2.NLRC5). See Supplementary Table 1 for a full list of differentially expressed genes and Supplementary Table 6 for description of devil-specific genes (LOC symbols).

884
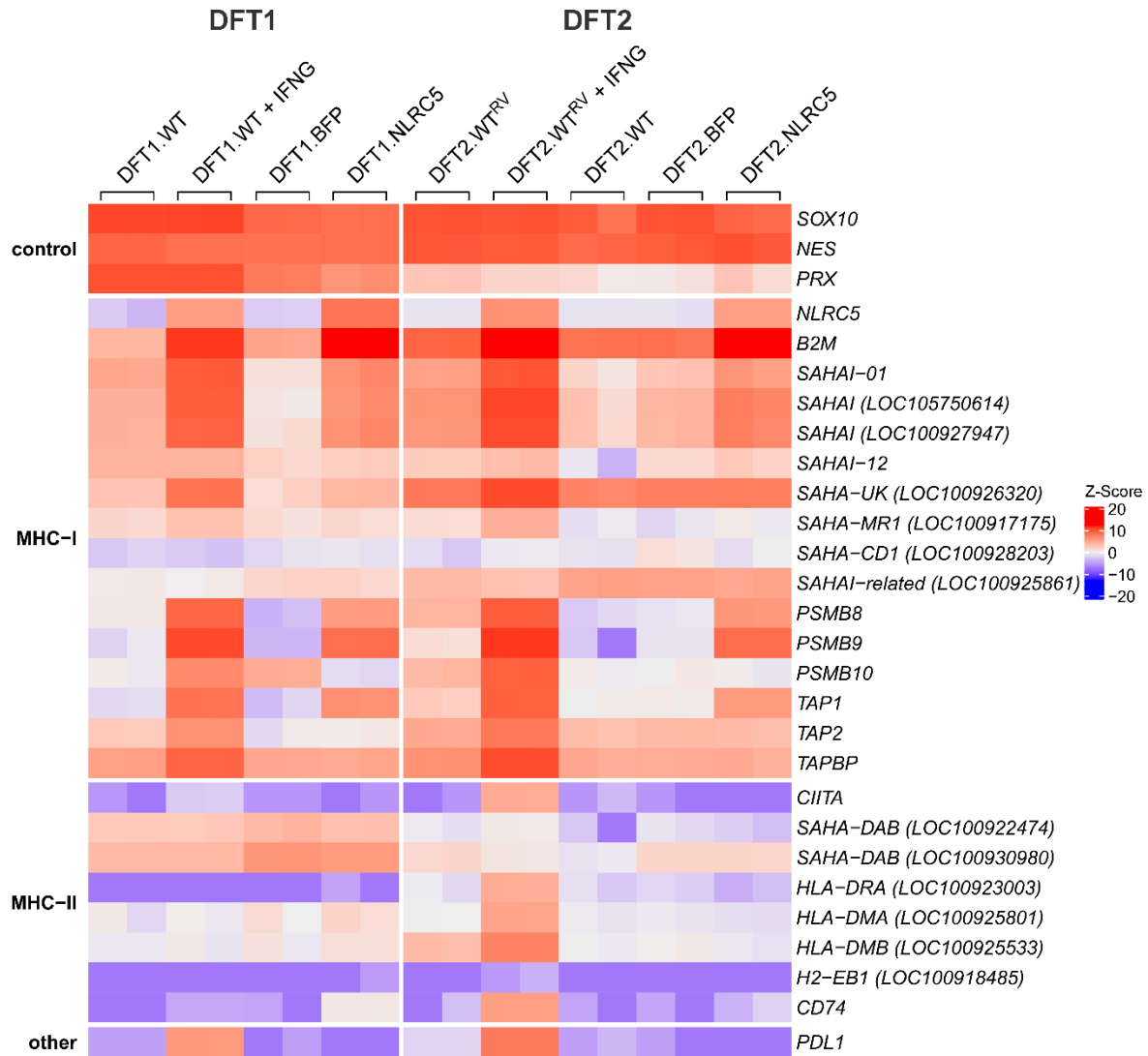
Figure 3. Heatmap showing expression profiles of genes involved in MHC-I and MHC-II antigen processing and presentation pathways, and PDL1 in IFNG-treated, and NLRC5-overexpressing DFT1 and DFT2 cells. Log$_2$TPM expression values were scaled across each gene (rows) and represented by Z-Score, with red and blue representing high and low relative expression, respectively. Replicates for each treatment (*N*=2) are included in the heatmap. *SAHAI* encodes the Tasmanian devil MHC-I heavy chain gene. For genes with no official gene symbol (LOC symbols), alternative gene symbols were used according to the gene description on NCBI. See Supplementary Table 6 for corresponding NCBI gene symbols and description.
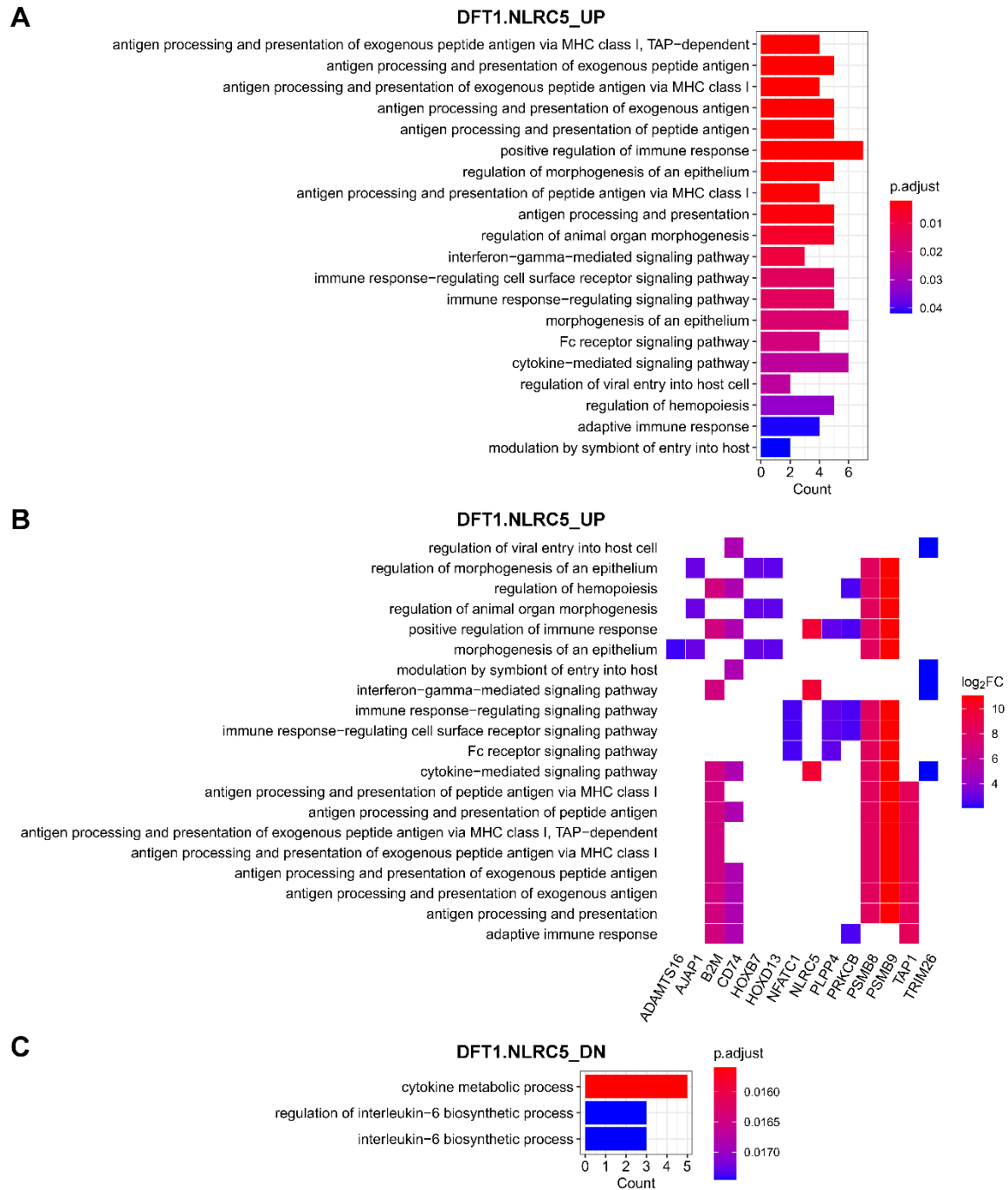
Figure 4. GO biological processes that were enriched in DFT1 cells with NLRC5 overexpression. GO biological process terms associated with genes upregulated (UP) **(A, B)** and downregulated (DN) **(C)** in DFT1.NLRC5. **(B)** Heatplot of genes associated with each positively-regulated GO term. The cut-offs p-value < 0.001 and adjusted p-value (p.adjust) < 0.05 were used to determine significant biological processes. P values were adjusted for multiple testing using Benjamini–Hochberg method. See also Supplementary Table 7 for full list of GO biological processes.
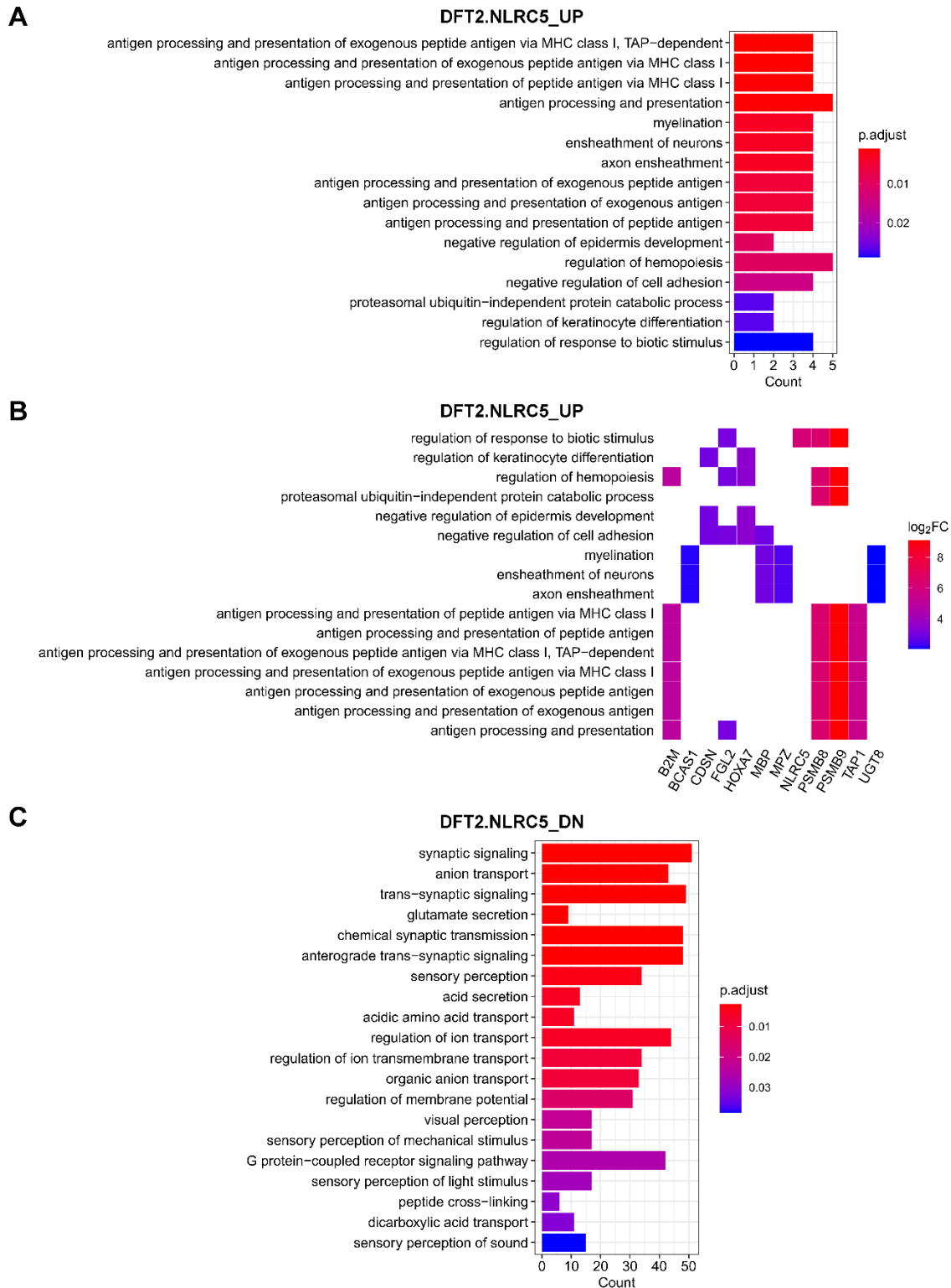
Figure 5. GO biological processes that were enriched in DFT2 cells with NLRC5 overexpression. GO biological process terms associated with genes upregulated (UP) **(A, B)** and downregulated (DN) **(C)** in DFT2.NLRC5. **(B)** Heatplot of genes associated with each positively-regulated GO term. The cut-offs p-value < 0.001 and adjusted p-value (p.adjust) < 0.05 were used to determine significant biological processes. P values were adjusted for multiple testing using Benjamini–Hochberg method. See also Supplementary Table 8 for full list of GO biological processes.

35

909
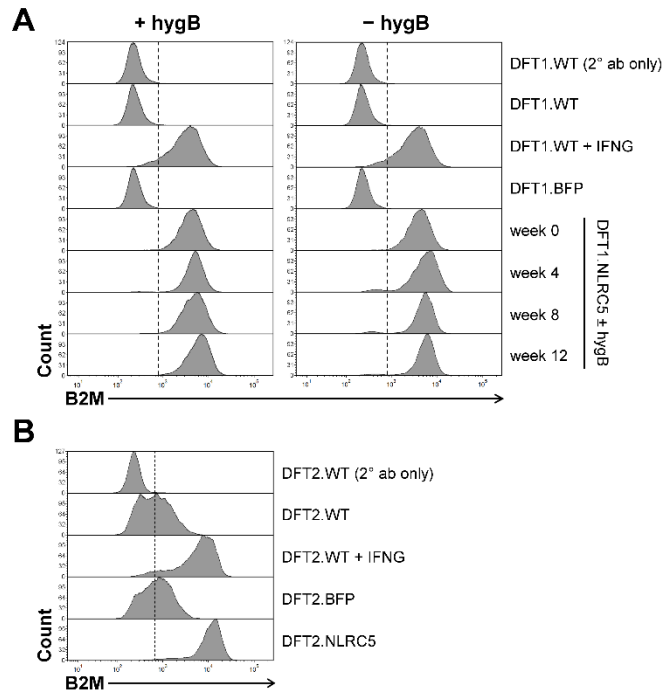
Figure 6. **Upregulation of MHC-I following NLRC5 overexpression.** Surface expression of B2M in DFT1.NLRC5 **(A)** and DFT2.NLRC5 **(B)**. B2M expression in the NLRC5 cell lines were compared to wild-type (DFT.WT), BFP-control (DFT.BFP), and IFNG-treated (DFT.WT + IFNG) DFT cells. **(A)** Stable expression of B2M in DFT1.NLRC5 was assessed every four weeks for 12 weeks post-drug selection in the presence and absence of hygromycin B (hygB) selection pressure. Secondary antibody-only staining (DFT.WT (2° ab only)) was included as a control. The results shown are representative of $N = 3$ replicates/treatment.
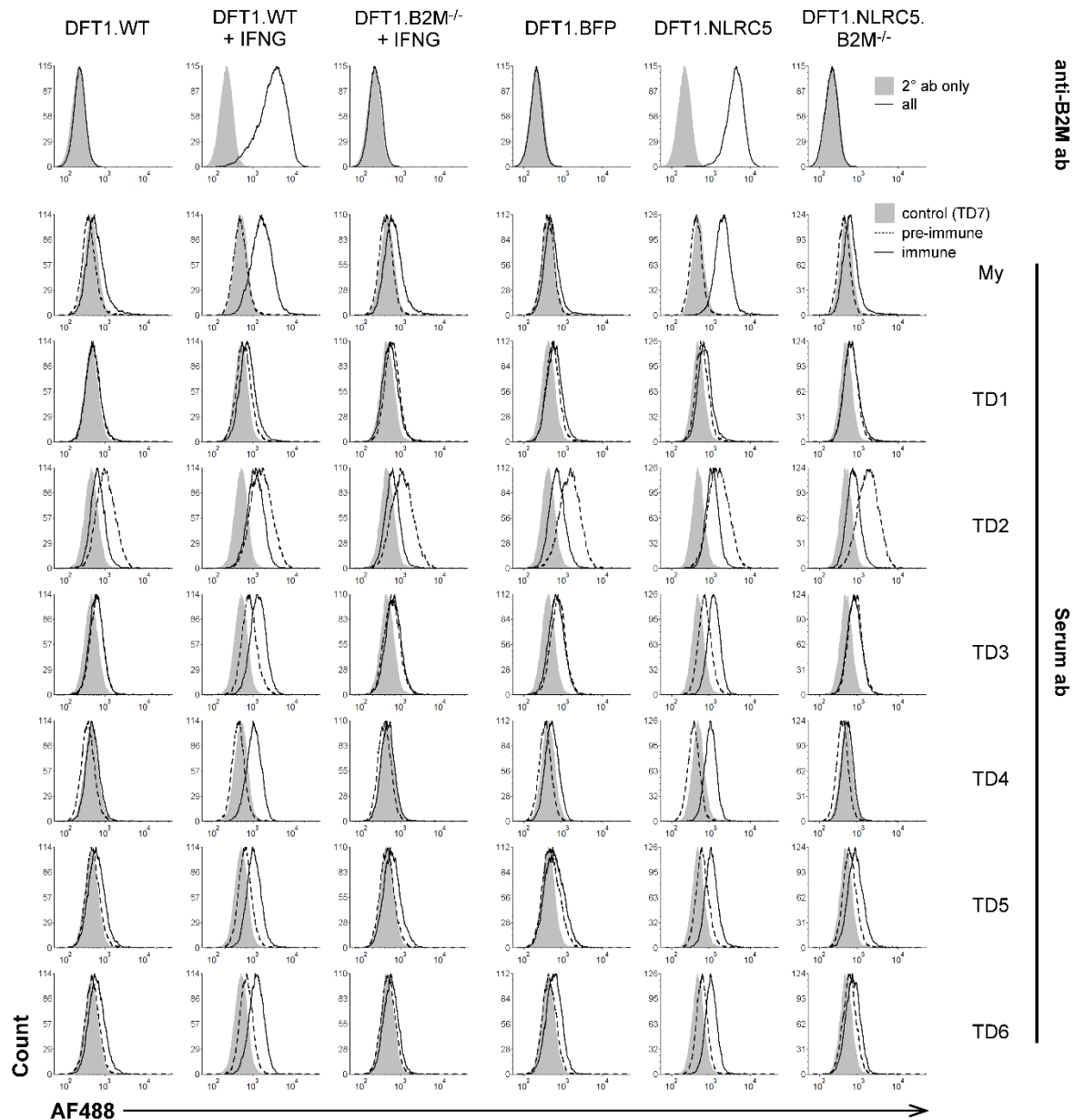
Figure 7. Flow cytometric analysis of serum antibody binding from devils with anti-DFT1 antibody response. Ablation of surface B2M in CRISPR/Cas9-mediated *B2M* knockout cells (B2M$^{-/-}$) was confirmed using a monoclonal anti-B2M antibody (anti-B2M ab). Sera from six devils (TD1-TD6) with seroconversion (immune) following DFTD infection were tested against wild-type DFT1 (DFT1.WT), IFNG-treated DFT1 (DFT1.WT + IFNG), IFNG-treated *B2M* knockout DFT1 (DFT1.B2M$^{-/-}$ + IFNG), BFP-control (DFT1.BFP), DFT1 overexpressing NLRC5 (DFT1.NLRC5) and *B2M* knockout NLRC5-overexpressing DFT1 (DFT1.NLRC5.B2M$^{-/-}$) cells. An immunized devil with induced tumor regression (My) was included as a positive control, meanwhile serum from a healthy devil (TD7) was included as a negative control as represented in the shaded grey area. *Ab*, antibody; *AF488*, Alexa Fluor 488.

37